Chinese Journal of Chemical Engineering 56 (2023) 89–96

Contents lists available at ScienceDirect

Chinese Journal of Chemical Engineering

journal homepage: www.elsevier.com/locate/CJChE

Full Length Article

Polymeric assembled nanoparticles through kinetic stabilization by confined impingement jets dilution mixer for fluorescence switching imaging

Jingran Liu [1], Yue Wu [1], Jie Tang [1], Tao Wang [1], Feng Ni [2], Qiumin Wu [1], Xijiao Yang [1], Ayyaz Ahmad [3], Naveed Ramzan [4], Yisheng Xu [1,*]

[1] State Key Laboratory of Chemical Engineering, East China University of Science and Technology, Shanghai 200237, China
[2] Shanghai Shyndec Pharmaceutical Co., Ltd, Shanghai 200040, China
[3] Department of Chemical Engineering, Muhammad Nawaz Sharif University of Engineering and Technology, Multan, Pakistan
[4] Faculty of Chemical, Metallurgical, and Polymer Engineering, University of Engineering & Technology, Lahore, Pakistan

ARTICLE INFO

Article history:
Received 8 March 2022
Received in revised form 12 June 2022
Accepted 13 June 2022
Available online 13 September 2022

Keywords:
Preparation
Kinetic stabilization
Flash nanoprecipitation
Nanoparticles
Fluorescence switch

ABSTRACT

Traditional fluorescence switching molecules achieving the state change between on and off states commonly based on UV irradiation. However, it is worth noting that UV irradiation is harmful to both the cancer cells and the normal cells. To achieve fluorescence switching under visible wavelength and avoid complicate molecular design, a fluorophore of 2,4,5,6-tetrakis(carbazol-9-yl)-1,3-dicyanobenzene (4CzIPN) and a quencher of diarylethene (DAE) were physically incorporated within the biocompatible block copolymer poly(lactic-co-glycolic acid)-*b*-poly(ethylene glycol) (PLGA-*b*-PEG) to form 4CzIPN-DAE nanoparticles (NPs) through flash nanoprecipitation (FNP). By using the FNP method, the NPs were prepared within milliseconds in a confined impingement jets dilution (CIJ-D) mixer. Quenching and recovery of fluorescence could achieve in the presence of DAE under 475 nm and 560 nm irradiation. Appropriate structure and fluorescent properties of the nanoparticles can be tuned by external conditions for their efficient fluorescence resonance energy transfer (FRET) in a kinetic stabilization process. This NPs formation process was further optimized by varying the dilution ratio, Reynolds number (*Re*) and polymer concentration to modulate the mixing and particle nucleation and growth process. The size and fluorescence switching properties of the NPs were systematically investigated in solution and in cellular uptake experiments. This work is anticipated to provide a simple and highly effective engineering strategy for the modulation of fluorescence switching nanoparticles and beneficial to its engineering application.

1. Introduction

Cell imaging plays an important role in cancer diagnosis, and compared to other imaging methods, such as magnetic resonance imaging and etc, fluorescence imaging is a general imaging strategy [1]. It features non-invasive, high sensitivity and resolution imaging, which makes it promising in the development of novel and practical imaging technology [2]. However, conventional fluorescent dyes for fluorescent imaging are useful for cellular studies but the fluorescence response is irreversible. And thus their practical application was limited by fluorescence background, optical diffraction limitation and so on [3]. In contrast, materials with good fluorescence reversibility provide a simple and effective protocol which could circumvent the above limitations [4–7]. Specifically, the system of combining photochromic materials with fluorophores showed good fluorescence reversibility [7–9]. Fluorescence switching nanoparticles based on this system have attracted a great deal of interest in recent years because of their potential application in optical data storage and super resolution imaging, *etc.* [6,7,10–13]. Among of all these photochromic molecules, diarylethene (DAE) is a promising photoswitch which features excellent fatigue, thermal stability and rapid response [11,14]. Plenty of efforts have been put into the development of fluorescence switching nanoparticles based on DAE. Su and coworkers[10] prepared organic nanoparticles based on the system

* Corresponding author.
E-mail address: yshxu@ecust.edu.cn (Y. Xu).

https://doi.org/10.1016/j.cjche.2022.06.034
1004-9541/

of a DAE derivative and the dye of benzothiadiazole (BTD) where they are covalently linked. With the good overlap between absorption spectra of the closed state of DAE and emission spectra of BTD, fluorescence reversibility of nanoparticles could be achieved by fluorescence resonance energy transfer (FRET) under UV and visible light and it could be repeated many times. Diarylethene-perylenebisimide (DAE-PBI) dyad was also chemically synthesized and fluorescence switching nanoparticles based on this system were prepared by traditional reprecipitation method [15]. The nanoparticles with enhanced photostability showed good fluorescence quenching and recovery under UV and visible light. Besides, emulsion polymerization strategy was also used to prepare fluorescence switching polymer nanoparticles based on the fluorescent materials and DAE, and the nanoparticles displayed fluorescence modulation in solution and living cells [16]. These nanoparticles are promising in the development of high fluorescence reversibility materials and fluorescence imaging technology. While majority of work mostly involves the chemical structural design which is a complicated and time-consuming process to delicate control the energy transfer between the fluorophores and photo switchers [4,5,17]. And often followed complex preparation method. However, complicated chemical structural design and tedious preparation were not anticipated in these studies. Therefore, easily operated and time-saving methods avoiding molecular structure design for the preparation of fluorescent nanoparticles are very helpful for practical clinic applications.

Plenty of methods were used for nanoparticle preparation but were time-consuming and not easily operated as described before. Flash nanoprecipitation (FNP) with advantages of fast mixing and processing, simple setup, controllable size and size distribution of particles was proposed to solve these problems [18,19]. FNP process has been used for preparation of nanomaterials in various fields, such as drug delivery [20–24], bio-imaging [25,26], catalysis [27,28], *etc*. FNP combines rapid mixing technique between solvent and antisolvent with nucleation and growth of hydrophobic molecules and amphiphilic polymer in microscale to form kinetically frozen nanoparticles [29] Mixers based on FNP were also studied before, such as confined impingement jets dilution (CIJ-D) mixer [30,31], multi-inlet vortex mixer (MIVM) [21,24,32,33], and microfluidic mixer [34]. The two fluid streams in completely opposing direction were drove to collide at high velocity for CIJ-D mixer, where turbulent mixing happened [34]. In the CIJ-D mixer, the addition of a dilution process after rapid mixing leads to rapid quenching with high volume of antisolvent which enhances stability of nanoparticles. CIJ-D mixer has a simple setup, which is easy to operate and avoids waste of materials [22]. More importantly, the size and inner structure could be finely tuned by external factors [20,35] including dilution ratio, flow rate, and polymer concentration. This potentially offers a good opportunity to adjust size distribution and fluorescent properties of nanoparticles (NPs) for efficient fluorescence reversibility. In fact, fluorescence switching nanoparticles encapsulating FRET pairs for monitoring nanoparticles *in vitro* and *in vivo* have been studied before [9]. However, tunable size and fluorescent properties of fluorescence switching nanoparticles were rarely focused but it is important to understand the relationship between nanoparticle structure and FRET process.

In this work, photochromic DAE acted as the photo-switcher, while 2,4,5,6-tetrakis(carbazol-9-yl)-1,3-dicyanobenzene (4CzIPN) acted as the fluorescent molecule. Poly (lactic-co-glycolic acid)-*b*-poly (ethylene glycol) (PLGA-*b*-PEG) FDA approved features non-cytotoxic and good compatibility was chosen as the stabilizer. As schemed in Fig. 1(a) and (b), when two impingent streams collided in a confined space, turbulent mixing at microscale was generated to afford supersaturation of 4CzIPN and DAE together in millisecond scale for nucleation and growth, where size distribution and fluorescent properties of nanoparticles can be tuned by adjusting the time of mixing (τ_{mix}) and nucleation and growth (τ_{flash}). The behaviors of fluorescence quenching and recovery of 4CzIPN-DAE NPs could be well achieved under 475 nm and 560 nm (Fig. 1(c)). The NPs formation process and its properties was optimized by varying process parameters. This work is promising to provide a more effective engineering strategy for the preparation and modulation of fluorescence switching nanoparticles.

2. Materials and Methods

2.1. Materials

PLGA10k-*b*-PEG5k were purchased from Yarebio, DAE was synthesized according to previous work [36], 4CzIPN was purchased from Xi'an Polymer Light Technology Corp. Tetrahydrofuran (THF, AR $\geq$ 99.5%) was purchased from general-reagent. 3-(4,5-Dimethyl thiazol-2-yl)-2,5-diphenyltetrazolium bromide (MTT) was purchased from KeyGEN. Dulbecco's modified Eagle's medium (DMEM) and phosphate buffered saline (PBS) were purchased from Hyclone. Fetal bovine serum (FBS) and penicillin–streptomycin liquid was purchased from Gibco. Dimethyl sulfoxide (DMSO) was purchased from Macklin. Potassium dihydrogen phosphate, potassium chloride and sodium chloride of analytical grade were purchased from general-reagent. Sodium phosphate dibasic dodecahydrate of analytical grade was obtained from Aladdin. Ultrapure water was used in all experiments.

2.2. Preparation of NPs

The typical procedure for particle preparation using the CIJ-D mixer was shown in Fig. 1. For the solvent stream, DAE, 4CzIPN with the same mole ratio, and the amphiphilic polymer PLGA-*b*-PEG were dissolved in THF. PBS with pH of 7.4 acted as the antisolvent stream. The exit stream was submerged in PBS (pH = 7.4). The two syringes with equal volume were then pushed rapidly by pump (Harvard Apparatus, PHD 2000 programmable) to inject the liquids into the CIJ-D mixer at the equal flow rates, where the two streams were vigorously mixed. The final NPs suspension was dialyzed against PBS (pH = 7.4) for 24 h to remove THF completely before characterization.

2.3. Characterizations of NPs.

A NICOMP 380 ZLS instrument was used to measure the hydrodynamic diameter, size distribution (polydispersity index, PDI) of nanoparticles. The angle of measurement was fixed at 90°. A JEOL JEM-2100 transmission electron microscope (TEM) with an acceleration voltage of 120 kV was used to observe the morphology of nanoparticles. The sample was prepared by depositing 20 μl of nanosuspension on a copper grid and dried in air. The fluorescence spectra were obtained using a F97PRO with 900 V PMT voltage with an excitation wavelength of 365 nm. The concentration and encapsulation efficiency [37] of 4CzIPN were determined by UV1800 analysis.

2.4. In vitro cytotoxicity assay

The human epithelioid cervical carcinoma cell line Hela cells were provided by the State Key Laboratory of Chemical Engineering of the East China University of Science and Technology. They were propagated in dishes cultured at 37 °C under a humidified 5% CO_2 atmosphere in Hyclone medium supplemented with 10% FBS and 1% penicillin–streptomycin.

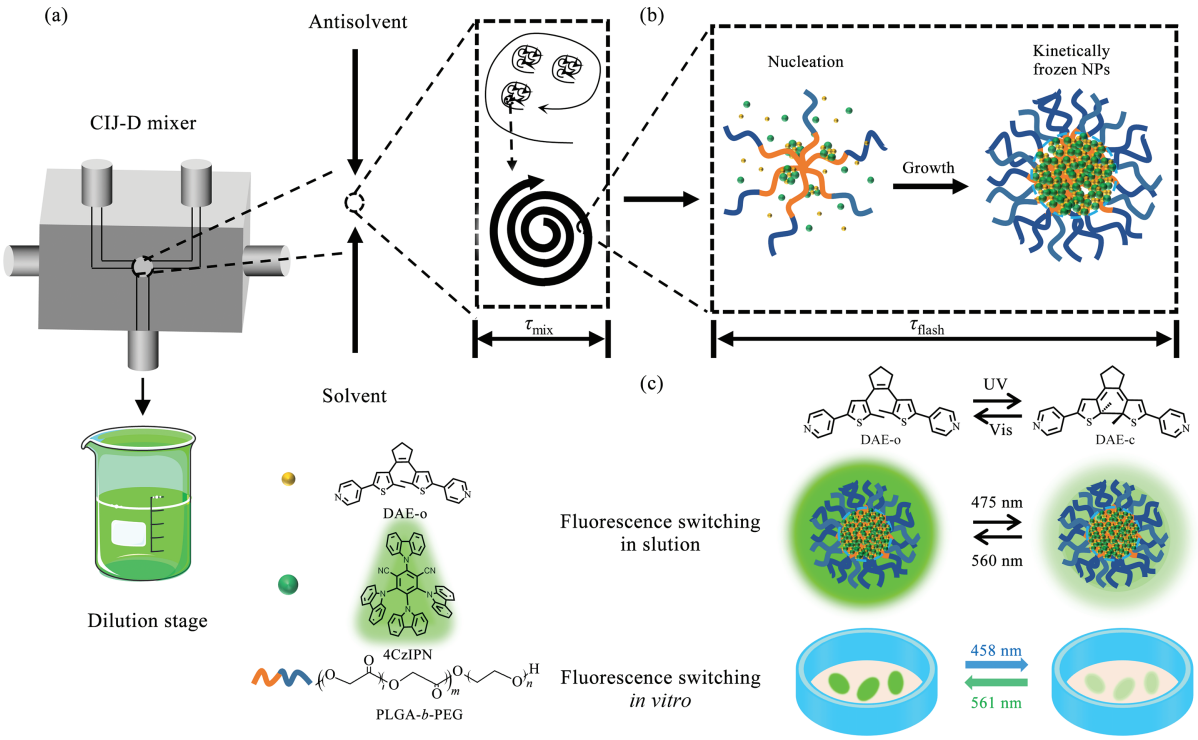

Fig. 1. Schematic illustration of (a) flash nanoprecipitation process with CIJ-D mixer and rapid mixing between two streams; (b) process of nucleation, growth of hydrophobic molecules and amphiphilic polymer. (c) Photo switch of DAE without 4CzIPN, fluorescence quenching and recovery of 4CzIPN-DAE NPs in solution and *in vitro*.

The cytotoxicity of NPs using Hela cells was measured by MTT assay [35]. Cells were plated in 96-well plates in 100 μl volume of DMEM medium with 10% FBS and 1% penicillin–streptomycin, at a density of 5×10^3 cells/well. After incubation for 24 h, the previous medium was removed, and the fresh medium containing different concentrations of 4CzIPN-DAE NPs was added. 20 μl MTT was directly added to each well after incubation for a certain time, and then cultured with cells at 37 °C under a humidified 5% CO_2 atmosphere for 4 h. The previous medium was removed and 150 μl DMSO was then added. The absorbance of solution was measured at 490 nm. Each sample was measured in triplicate.

2.5. Confocal fluorescence imaging for living cells.

1.0 ml of DMEM containing Hela cells were plated onto glass-bottom dish and allowed to adhere for 24 h before treatment. The previous medium was removed, cells were then exposed to different 4CzIPN concentrations of NPs solutions, and incubated for several h at 37 °C under a humidified 5% CO_2 atmosphere. After that, the cells were washed by PBS for three times and the 1.0 ml fresh medium was added. Fluorescence imaging was then performed using a confocal laser scanning microscope (CLSM, Leica SP8) with a 40× objective lens. The fluorescence signals were collected at 468–518 nm, using a laser at 458 nm as excitation light source.

3. Results and Discussion

3.1. Preparation of fluorescence switching NPs

The chemical structures of the hydrophobic molecules and stabilized copolymer were shown in Fig. 1(a). 4CzIPN with a ACDLogP [38] (calculated by freeware ACD/Chemsketch and used for the prediction of hydrophobicity) around 16.74 is a fluorescent molecule, and DAE with a ACDLogP around 7.49 is a photo switchable molecule. The amphiphilic block polymer, PLGA-*b*-PEG, featuring biocompatible, biodegradable and nontoxic, is used for the stabilizer to prepare fluorescence switching NPs. CIJ-D mixer is an ideal device by providing two impingent flows to create microscale mixing for two hydrophobic molecules assembly simultaneously [30].

The size, morphology and fluorescent intensity have tremendous influence on the efficiency of cellular uptake. It has been reported that the diameter of 100 nm nanoparticles exhibit much greater uptake compared to 1 μm and 10 μm particles [39]. As shown in Fig. 2(a), the size of NPs produced by FNP was 152 nm with a PDI of 0.152 characterized by dynamic light scattering (DLS). The corresponding TEM image indicated that the morphology of NPs was spherical (Fig. 2(b)), with a mean diameter of 138 nm. The 4CzIPN and DAE were intermingle with the PLGA block of the amphiphilic copolymer, which were in turn surrounded by the hydrophilic PEG corona. The PEG corona was not visible in TEM because of its low contrast [21,40], which explains the diameter characterized by TEM was a little smaller than the data of DLS [24]. The absorbance and fluorescence spectra of the NPs were shown in Fig. 2(c) and 2(d), the open ring isomer of DAE (DAE-o) has obvious photochromism in aqueous phase. Irradiation of DAE-o with 475 nm light led to a new absorption at 560 nm in the presence of 4CzIPN (Fig. 2(c)), accompanied by quenching around 75% of the fluorescence of 4CzIPN within 120 s in photo stationary state (PSS) as presented in Fig. 2(d). The fluorescence spectra of 4CzIPN partially overlaps with the absorption of DAE in the closed-ring isomer (DAE-c), which resulted in strong energy transfer from the energy donor (4CzIPN) to the acceptor (DAE-c), while the absorption spectra of DAE-o showed no overlap. From these spectra properties, it is expected that only DAE-c could work as a fluorescence quencher for 4CzIPN. Under 560 nm light irradiation, both absorption and fluorescence of 4CzIPN-DAE NPs almost completely recovered to the spectra before 475 nm irradiation according to the spectral change

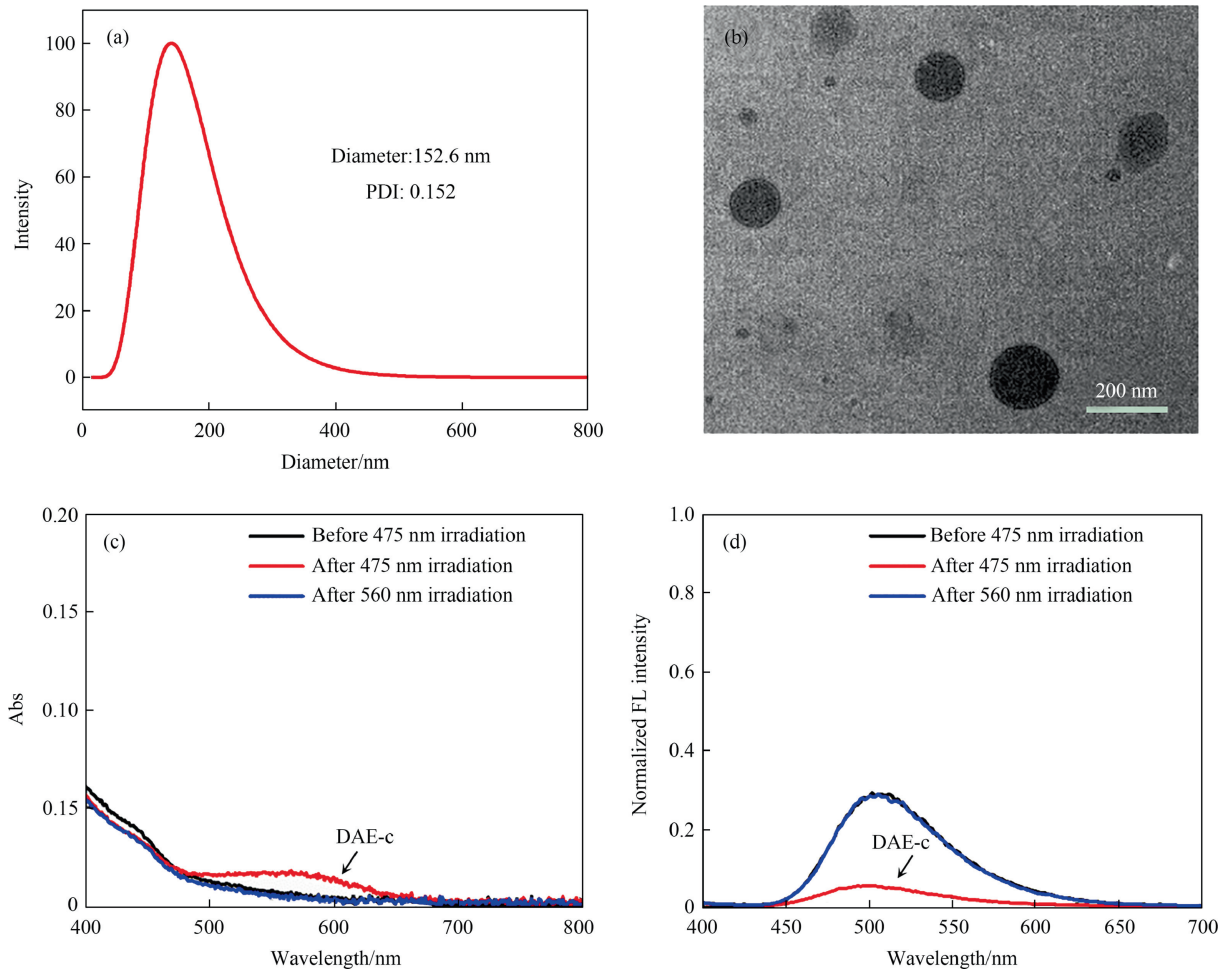

Fig. 2. (a) Diameter, PDI and (b) TEM image of 4CzIPN-DAE NPs. (c) The corresponding absorption and (d) fluorescence spectra of 4CzIPN-DAE NPs in PBS solution (λ_{ex} = 365 nm). Experimental conditions: DAE: 0.1 mg·ml^{-1}, 4CzIPN: 0.19 mg·ml^{-1}, $PLGA_{10k}$-*b*-PEG_{5k}: 2.5 mg·ml^{-1}, *Re*: 4356, dilution ratio (dilution ratio represents the volume of PBS used to dilute/the volume of THF): 18.

(Fig. 2(c) and 2(d)), showing the classical switchable property of DAE. It was demonstrated that such water "soluble" fluorescence switching NPs, which integrated two isolated hydrophobic molecules into a single nanoparticle, thus provide an ideal platform for application in super resolution imaging owing to their good fluorescence reversibility in water. The fluorescence switching behaviors and size of the NPs strongly depend on the external factors during the FNP process, which are needed to be carefully considered, such as dilution ratio, flow rate and polymer concentration.

3.2. Influence of dilution ratio

As shown in Fig. 3(a) and (b), when the volume of the dilution stage (*i.e.*, the volume of PBS in outlet beaker) was changed from 4.5 ml to 27 ml corresponding to the change of dilution ratio (the volume of PBS used to dilute/the volume of THF) from 3 to 18, all 4CzIPN-DAE NPs exhibited particle sizes about 80 nm with PDI below 0.3 characterized by DLS. Fig. 3(c) indicated that the fluorescence intensity was almost constant at different dilution ratios. It might be that partial 4CzIPN molecules of 4CzIPN-DAE NPs prepared at a low dilution ratio dissolved in the organic phase, which were removed through dialysis leading to the concentration of 4CzIPN decreasing and the fluorescence intensity decreasing [41]. Therefore, the fluorescence intensity remained almost the same at different dilution ratios. For CIJ-D mixer, the subsequent dilution process with high volume of antisolvent leads to rapid quenching that enhances nanoparticle stability to some extent [30]. PLGA-*b*-PEG, which was also studied with a glass transition temperature (T_g) of PLGA above room temperature, has a larger difference in solubility with PEG and PLGA, thus less PEG to be trapped in the internal structure of an amphiphilic polymer based nanoparticle, resulting in higher PEG surface coverage and greater stability [40]. As shown in Fig. 3(d), these particles showed good long-term (~14 d) stability.

3.3. Influence of flow rate

The effect of flow rate reflected by the Reynolds number (*Re*) was further investigated. Han *et al.* [30] investigated and finally confirmed that that higher *Re* was related with more efficient mixing. The *Re* in the present mixing system was defined as follows [30].

$$Re = \sum_{i=1}^{n} Re_i = \frac{4}{\pi d} \sum_{i=1}^{n} \frac{\rho_i Q_i}{\mu_i} \quad (1)$$

where ρ_i is the density of the fluid (kg·m^{-3}); Q_i is the volumetric flow rate of the inlet stream (m^3·s^{-1}); μ_i is the viscosity of the fluid (Pa·s); d is the stream inlet diameter (m), which is the same for the two inlet streams. The Reynolds number calculated according to Eq. (1) by changing the flow rates of the two streams was shown in Table S1 (in Supplementary Material).

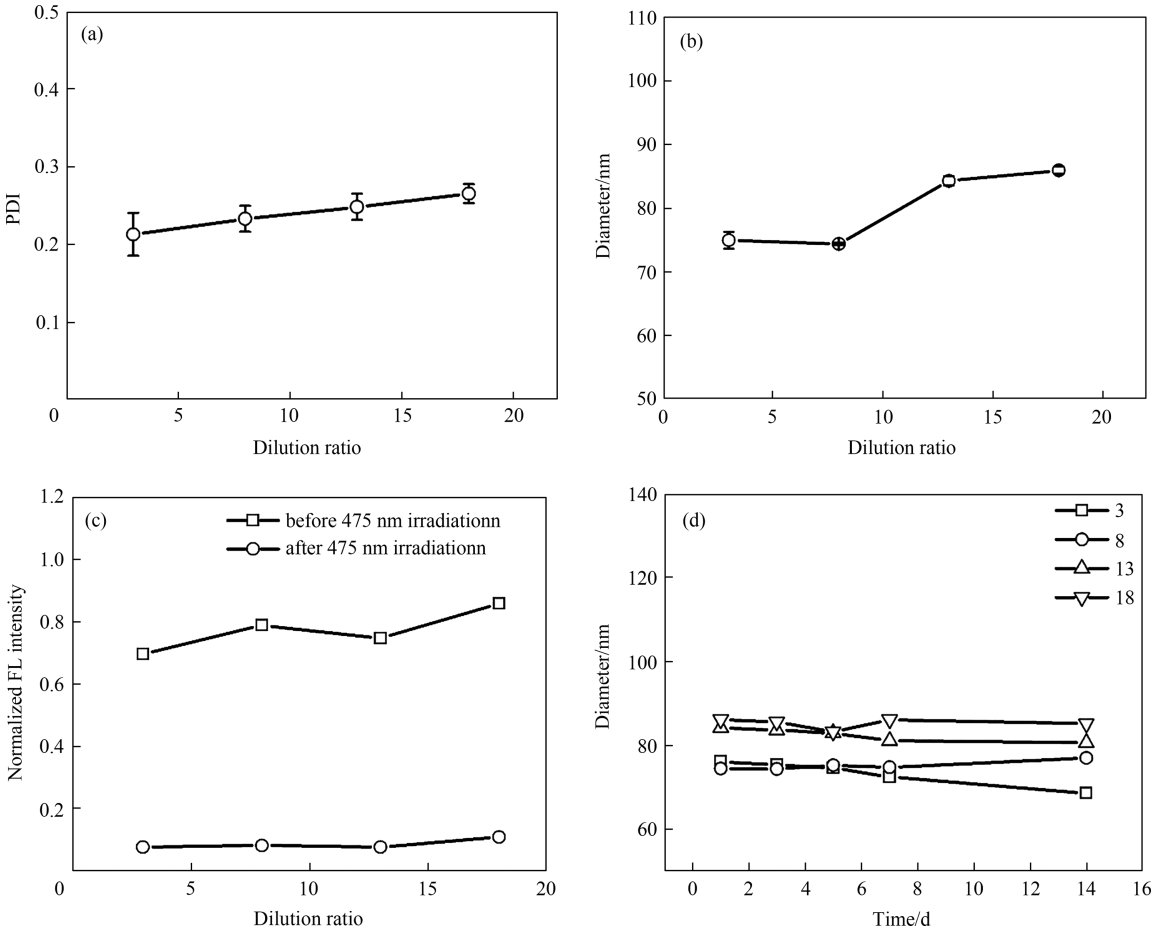

Fig. 3. (a) Size, (b) PDI, (c) normalized FL intensity and (d) stability of 4CzIPN-DAE NPs prepared at different dilution ratios (the volume of PBS used to dilute/the volume of THF) after dialysis. Experimental conditions: DAE: 0.1 mg·ml^{-1}, 4CzIPN: 0.19 mg·ml^{-1}, PLGA$_{10k}$-*b*-PEG$_{5k}$: 5.0 mg·ml^{-1}, *Re*: 4356.

It was shown that the size of the nanoparticles reduced from 140 nm to 80 nm upon increasing *Re* from 726 to 6660 as indicated in Fig. 4(a). As the mixing time became shorter accompanied by higher *Re* within the mixer, the mixed fluid performed much more homogeneous and effective mixing [18]. Therefore, when *Re* was increased at first, the ratio of τ_{mix}/τ_{flash} was much larger than 1 and the size of 4CzIPN-DAE NPs decreased greatly. However, it was noted that size of nanoparticles didn't change even if *Re* increased when *Re* was larger than 4356, hence *Re* was kept at 4356 in the subsequent studies. This phenomenon corresponds to the facts that when the ratio of τ_{mix}/τ_{flash} was much less than 1, the critical particle size formed under homogeneous conditions [19]. Fig. 4(b) indicated the good stability of the nanoparticles at different *Re* values, which means 4CzIPN-DAE NPs prepared by FNP could be stable and suitable for different particle size requirements. Additionally, Fig. 4(c) showed that the fluorescence intensity remained constant under different *Re* values. This probably suggests that as the concentrations of 4CzIPN, DAE and PLGA-*b*-PEG were fixed, the compositions of two hydrophobic molecules were kept same in the final NP suspension.

3.4. Influence of polymer concentration

The effect of polymer concentration was then investigated. When the polymer concentration varied from 0.5 mg·ml^{-1} to 10 mg·ml^{-1} as shown in Fig. 5(a), the size of NPs decreased from 220 nm to 120 nm. This can be explained by the competition between solute nucleation and growth and polymer aggregation/stabilization during FNP process [18,19]. In the FNP process, hydrophobic block of the polymer and hydrophobic molecules were nucleated simultaneously to form nucleus and then grew, while the polymer aggregated and stabilized the nucleus forming nanoparticles [18]. The precipitation time of PLGA-*b*-PEG became shorter under higher polymer concentration [19] and less aggregates formed the nucleus of nanoparticles leading to smaller nanoparticles. At low concentrations ($\leq$1 mg·ml^{-1}), the nanoparticles were unstable and started to aggregate (Fig. 5(b)) after one week due to the low surface coverage of PEG [19]. Fig. 5(c) showed the fluorescence intensity of 4CzIPN-DAE NPs before 475 nm irradiation increased almost ten times as the polymer concentration increased. The same phenomenon also happened in 4CzIPN NPs without DAE (Fig. S1). At higher polymer concentration, much smaller size of the nanoparticles were formed accompanied by much higher encapsulation efficiency of 4CzIPN (Table S2) which greatly enhanced the fluorescence intensity of the nanoparticles [41].

As shown in Fig. 6(a) and (b), fluorescence intensity can be quenched by 475 nm irradiation and can be reversed after 560 nm irradiation. Such reversibility was observed for 4CzIPN-DAE NPs at different PLGA-*b*-PEG concentrations. While the largest fluorescence intensity and contrast was observed for highest polymer concentrations at 10 mg·ml^{-1}. The polymer concentration of 1 mg·ml^{-1} and 10 mg·ml^{-1} were used to study the fluorescence reversibility. After 120 s irradiation at 475 nm, the fluorescence intensity of 4CzIPN can be mostly quenched and recovered completely after 560 nm irradiation for 180 s at both concentrations.

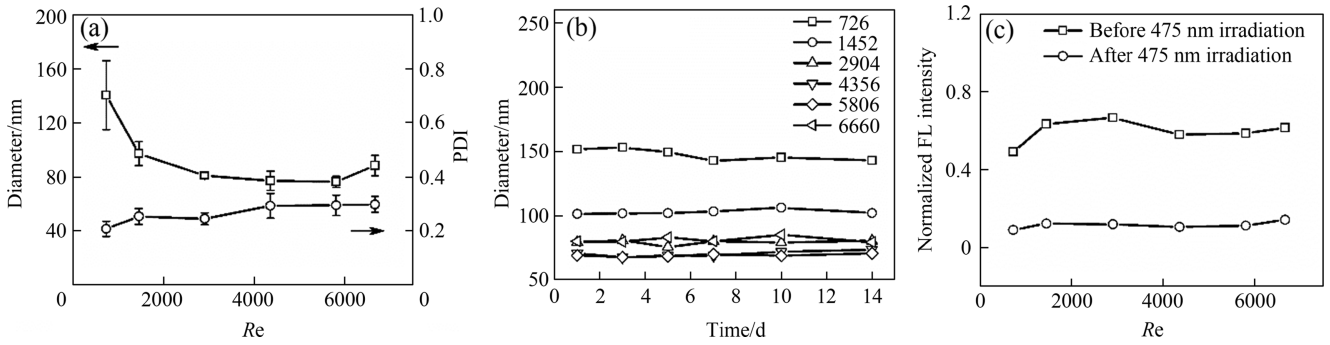

Fig. 4. (a) Size distribution, (b) stability and (c) normalized FL intensity of 4CzIPN-DAE NPs prepared at different *Re* values after dialysis. Experimental conditions: DAE: 0.1 mg·ml^{-1}, 4CzIPN: 0.19 mg·ml^{-1}, $PLGA_{10k}$-*b*-PEG_{5k}: 5.0 mg·ml^{-1}, dilution ratio: 18.

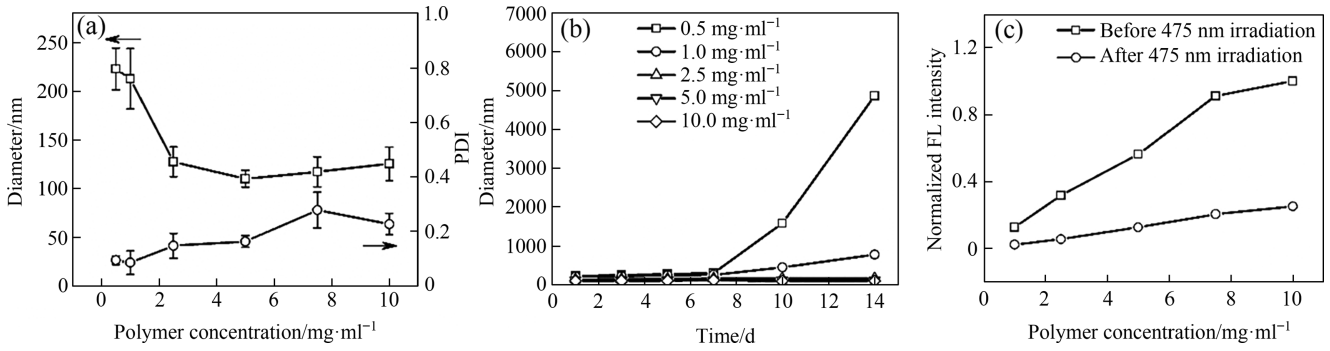

Fig. 5. (a) Size distribution, (b) stability and (c) normalized FL intensity of 4CzIPN-DAE NPs prepared at different polymer concentrations after dialysis. Experimental conditions: DAE: 0.1 mg·ml^{-1}, 4CzIPN: 0.19 mg·ml^{-1}, dilution ratio: 18, *Re*: 4356.

As shown in Fig. S2, the fluorescence intensity of 4CzIPN-DAE nanoparticles only decreased a little after twelve days' storage at room temperature, indicating little degradation of the nanoparticles. FRET efficiency was also calculated according to the Eq. (2) in the article [42]. (calculate based on Fig. 6(b)).

$$E = (1 - \mathrm{FDA/FD}) \times 100\% = (1 - 0.24/0.94) \times 100\% = 74.47\% \quad (2)$$

where F_D and F_{DA} were the fluorescence intensity of the donor in the absence and presence of acceptor.

3.5. Fluorescence reversibility in vitro

The cytotoxicity of 4CzIPN-DAE NPs were also evaluated *via* MTT assay. As shown in Fig. 7, the viabilities of Hela cells remained higher than 90% after 6 h and 24 h incubation with various concentrations of 4CzIPN-DAE NPs, revealing the low cytotoxicity of 4CzIPN-DAE NPs.

The nanoparticles also showed good stability in DMEM as shown in Fig. S3. The cellular uptake behaviors of 4CzIPN NPs were studied using HeLa cells as the cell line. As shown in Fig. S4, 4CzIPN NPs with a concentration of 4CzIPN (15 μmol·L^{-1}) were incubated

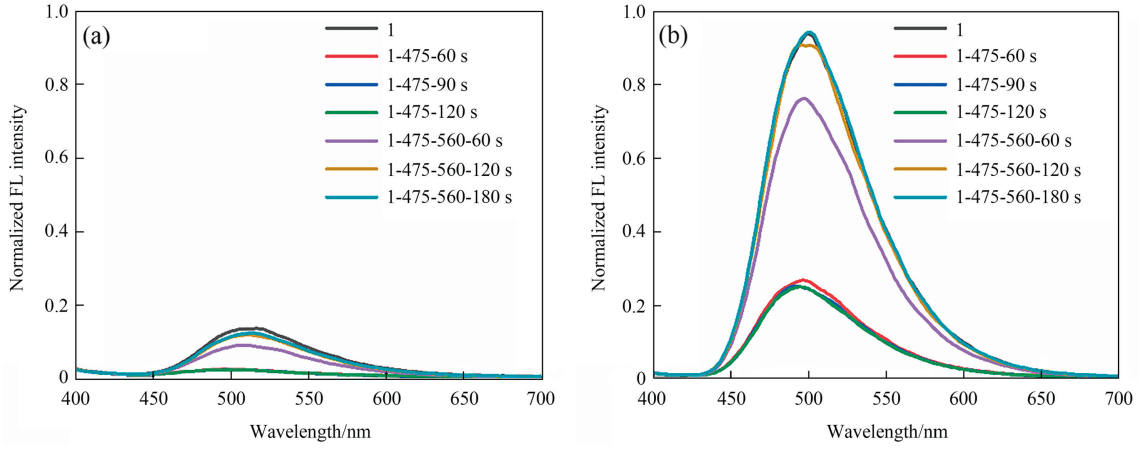

Fig. 6. Fluorescence spectra change of 4CzIPN-DAE NPs with the polymer concentration of (a) 1 mg·ml^{-1} and (b) 10 mg·ml^{-1} in PBS solution upon irradiation with 475 and 560 nm lights (λ_{ex} = 365 nm). Among of these, the black line (a) and (b) corresponded to the fluorescence intensity of 4CzIPN-DAE NPs before 475 nm irradiation. Experimental conditions: DAE: 0.1 mg·ml^{-1}, 4CzIPN: 0.19 mg·ml^{-1}, dilution ratio: 18, *Re*: 4356.

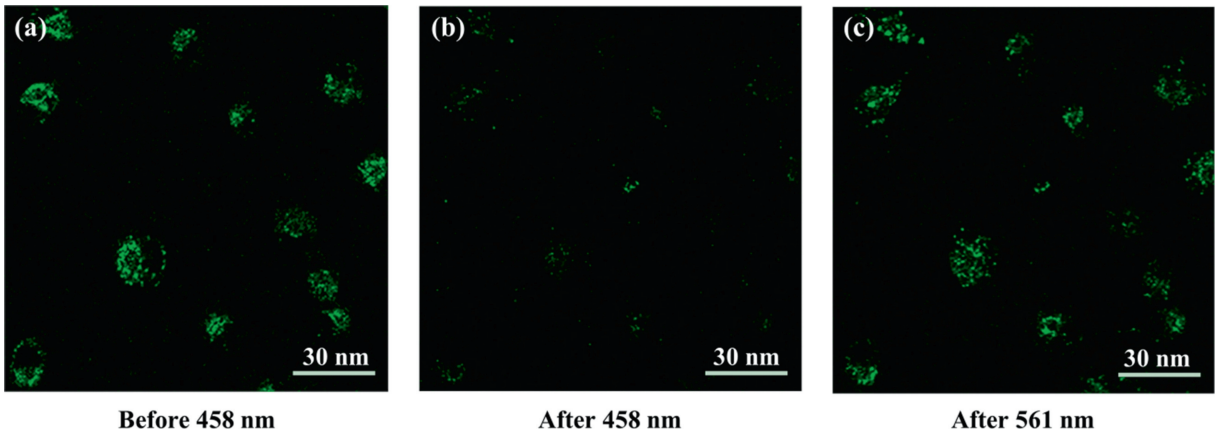

Fig. 8. Fluorescence image of Hela cells after 6 h incubation with 15 μmol·L^{-1} 4CzIPN-DAE NPs (a) before 458 nm irradiation; (b) 458 nm irradiation for 3 minutes; (c) 561 nm irradiation for 5 minutes after 458 nm irradiation. The signal was collected at 468–518 nm upon excitation at 458 nm. Experimental conditions: DAE: 0.5 mg·ml^{-1}, 4CzIPN: 0.95 mg·ml^{-1}, dilution ratio: 18, *Re*: 4356, $PLGA_{10k}$-*b*-PEG_{5k}: 10.0 mg·ml^{-1}.

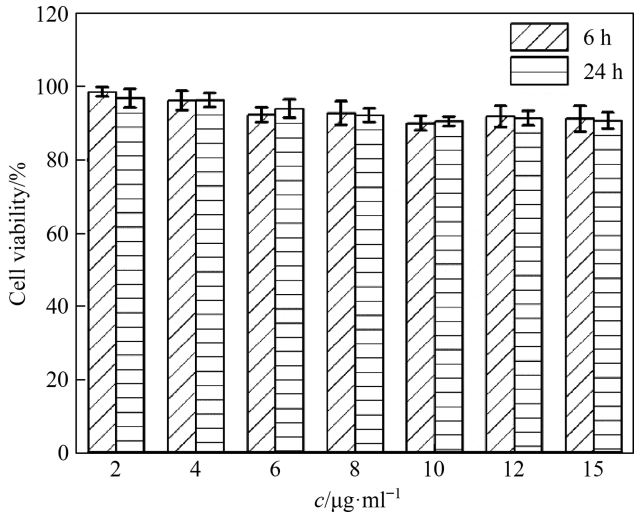

Fig. 7. Concentration-dependent cytotoxicity of 4CzIPN-DAE NPs after 6 and 24 h incubation. Experimental conditions: DAE: 0.5 mg·ml^{-1}, 4CzIPN: 0.95 mg·ml^{-1}, dilution ratio: 18, *Re*: 4356, $PLGA_{10k}$-*b*-PEG_{5k}: 10.0 mg·ml^{-1}.

with Hela cells for 6 h, CLSM was used to capture the fluorescence image. We can easily find that the fluorescence intensity remained the same after either 458 nm or 561 nm irradiation, which showed that fluorescence intensity of 4CzIPN remained same after different lights irradiation in the absence of DAE.

Inspired by the obvious fluorescence switching performance of 4CzIPN-DAE NPs in PBS solution, 4CzIPN-DAE NPs were then applied *in vitro*. The 4CzIPN-DAE NPs applied in cells were first characterized (Fig. S5) . The size of 4CzIPN-DAE NPs was 134.8 nm with PDI of 0.190. FRET efficiency could reach 81.58% calculated by Eq. (2). Fig. S6 showed that fluorescence intensity depended on the concentration of 4CzIPN, where 15 μmol·L^{-1} was found the most suitable concentration for cell imaging. Fig. 8 (a) showed that the fluorescence images of Hela cells treated with 4CzIPN-DAE NPs incubation for 6 h at 37 °C, which revealed a bright green fluorescence before 475 nm irradiation. It indicated that 4CzIPN-DAE NPs were internalized into Hela cells. After 458 nm irradiation for 3 min, fluorescence dramatically decreased as shown in Fig. 8(b) due to the photo induced ring closing process of DAE causing the fluorescence intensity quenching of 4CzIPN. The emission spectra of 4CzIPN and the absorption spectra of DAE-c overlapped to some extent, and the distance between 4CzIPN and DAE was less than 10 nm within the nucleus of NPs leading to FRET, resulting in the fluorescence of 4CzIPN ultimately quenching by DAE-c. After 561 nm irradiation for 5 minutes, the fluorescence of 4CzIPN gradually recovered because of the state change from DAE-c to DAE-o (Fig. 8(c)).

4. Conclusions

In conclusion, the fluorescent 4CzIPN and the photochromic DAE were physically encapsulated into a single NP *via* FNP for efficient switchable fluorescence response. The formed 4CzIPN-DAE NPs exhibited spherical morphology with size between 74 nm and 245 nm. The size distribution and fluorescence switching behaviors of 4CzIPN-DAE NPs could be easily controlled by micro-mixing conditions in a CIJ-D mixer by adjusting the dilution ratio, flow rate and polymer concentration. The fluorescence switching between on and off state were successfully demonstrated in PBS solution and in Hela cells. Quenching and recovery of 4CzIPN-DAE NPs could be successfully achieved under 475/458 nm and 560/561 nm lights irradiation in solution and vitro experiments. This work could provide opportunities for super-resolution imaging in the future.

Declaration of Competing Interest

The authors declare that they have no known competing financial interests or personal relationships that could have appeared to influence the work reported in this paper.

Acknowledgements

This work was financially supported by the National Key Research and Development Program of the International Scientific and Technological Innovation Cooperation Project among Governments (2021YFE0100400), Science and Technology Innovation Action Plan of Shanghai (22501100500), and the international One Belt One Road Collaboration Project of Shanghai (18490740300). The authors greatly thank Prof. A. Kayitmazer Basak at the Bogazici University for providing helpful discussions in the preparation process of NPs.

Supplementary Material

Supplementary data to this article can be found online at https://doi.org/10.1016/j.cjche.2022.06.034.

Nomenclature

d	stream inlet diameter, m
E	FRET efficiency,$E = (1 - \mathrm{FDA/FD}) \times 100\%$
F_D	fluorescence intensity of the donor in the absence of acceptor
F_DA	fluorescence intensity of the donor in the presence of acceptor
Q_i	volumetric flow rate of the inlet stream, $\mathrm{m^3 \cdot s^{-1}}$
Re	Reynolds number, $Re = \sum_{i=1}^{n} Re_i = \frac{4}{\pi d} \sum_{i=1}^{n} \frac{\rho_i Q_i}{\mu_i}$
T_g	glass transition temperature, °C
λ_ex	excitation wavelength, nm
μ_i	viscosity of the fluid, Pa·s
ρ_i	density of the fluid, $\mathrm{kg \cdot m^{-3}}$
τ_flash	time of nucleation and growth, s
τ_mix	time of mixing, s

References

[1] J.A. Barreto, W. O'Malley, M. Kubeil, B. Graham, H. Stephan, L. Spiccia, Nanomaterials: Applications in cancer imaging and therapy, *Adv. Mater.* 23 (12) (2011) H18–H40.

[2] M. Gao, F.B. Yu, C.J. Lv, J. Choo, L.X. Chen, Fluorescent chemical probes for accurate tumor diagnosis and targeting therapy, *Chem. Soc. Rev.* 46 (8) (2017) 2237–2271.

[3] G.X. Feng, D. Ding, K. Li, J. Liu, B. Liu, Reversible photoswitching conjugated polymer nanoparticles for cell and *ex vivo* tumor imaging, *Nanoscale* 6 (8) (2014) 4141–4147.

[4] Y. Zou, T. Yi, S.Z. Xiao, F.Y. Li, C.Y. Li, X. Gao, J.C. Wu, M.X. Yu, C.H. Huang, Amphiphilic diarylethene as a photoswitchable probe for imaging living cells, *J. Am. Chem. Soc.* 130 (47) (2008) 15750–15751.

[5] I. Yildiz, S. Impellizzeri, E. Deniz, B. McCaughan, J.F. Callan, F.M. Raymo, Supramolecular strategies to construct biocompatible and photoswitchable fluorescent assemblies, *J. Am. Chem. Soc.* 133 (4) (2011) 871–879.

[6] M.Q. Zhu, G.F. Zhang, Z. Hu, M.P. Aldred, C. Li, W.L. Gong, T. Chen, Z.L. Huang, S. Y. Liu, Reversible fluorescence switching of spiropyran-conjugated biodegradable nanoparticles for super-resolution fluorescence imaging, *Macromolecules* 47 (5) (2014) 1543–1552.

[7] K. Peng, F.T. Lv, H. Lu, J.W. Wang, H. Zhao, L.B. Liu, S. Wang, Conjugated polymer nanoparticles as fluorescence switch for selective cell imaging, *Chin. Chem. Lett.* 31 (3) (2020) 755–758.

[8] Z.Y. Li, C.J. He, Z.Q. Lu, P.S. Li, Y.P. Zhu, Recent progress in all-visible-light-triggered diarylethenes, *Dyes Pigments* 182 (2020) 108623.

[9] G.Z. Yang, Y. Liu, J.S. Teng, C.X. Zhao, FRET ratiometric nanoprobes for nanoparticle monitoring, *Biosensors* 11 (12) (2021) 505.

[10] J. Su, T. Fukaminato, J.P. Placial, T. Onodera, R. Suzuki, H. Oikawa, A. Brosseau, F. Brisset, R. Pansu, K. Nakatani, R. Métivier, Giant amplification of photoswitching by a few photons in fluorescent photochromic organic nanoparticles, *Angew. Chem. Int. Ed. Engl.* 55 (11) (2016) 3662–3666.

[11] T. Fukaminato, S. Ishida, R. Métivier, Photochromic fluorophores at the molecular and nanoparticle levels: Fundamentals and applications of diarylethenes, *NPG Asia Mater.* 10 (9) (2018) 859–881.

[12] Y.C. Yuan, H. Zhu, Y. Nagaoka, R. Tan, A.H. Davis, W.W. Zheng, O. Chen, Reversible photo-switching of dual-color fluorescent Mn-doped CdS-ZnS quantum dots modulated by diarylethene molecules, *Front. Chem.* 7 (2019) 145.

[13] M.L. Yu, P.S. Zhang, L. Liu, H. Wang, H. Wang, C.H. Zhang, Y. Gao, C.L. Yang, J.X. Cui, J. Chen, Reversibly photoswitchable tristate fluorescence within a single polymeric nanoparticle, *Adv. Opt. Mater.* 9 (22) (2021) 2101227.

[14] J.J. Zhang, H. Tian, The endeavor of diarylethenes: New structures, high performance, and bright future, *Adv. Opt. Mater.* 6 (6) (2018) 1701278.

[15] I. Ikariko, S. Deguchi, N. Fabre, S. Ishida, S. Kim, S. Kurihara, R. Métivier, T. Fukaminato, Highly-stable red-emissive photochromic nanoparticles based on a diarylethene-perylenebisimide dyad, *Dyes Pigments* 180 (2020) 108490.

[16] T.S. Yang, Q. Liu, S.Z. Pu, Z.S. Dong, C.H. Huang, F.Y. Li, Fluorophore-photochrome co-embedded polymer nanoparticles for photoswitchable fluorescence bioimaging, *Nano Res.* 5 (7) (2012) 494–503.

[17] M.Q. Zhu, L.Y. Zhu, J.J. Han, W.W. Wu, J.K. Hurst, A.D.Q. Li, Spiropyran-based photochromic polymer nanoparticles with optically switchable luminescence, *J. Am. Chem. Soc.* 128 (13) (2006) 4303–4309.

[18] B.K. Johnson, R.K. Prud'homme, Flash NanoPrecipitation of organic actives and block copolymers using a confined impinging jets mixer, *Aust. J. Chem.* 56 (10) (2003) 1021.

[19] B.K. Johnson, R.K. Prud'homme, Mechanism for rapid self-assembly of block copolymer nanoparticles, *Phys. Rev. Lett.* 91 (11) (2003) 118302.

[20] Z.N. Fu, L. Li, M.W. Wang, X.H. Guo, Size control of drug nanoparticles stabilized by mPEG-b-PCL during flash nanoprecipitation, *Colloid Polym. Sci.* 296 (5) (2018) 935–940.

[21] M.W. Wang, S. Lin, J.Y. Wang, L. Liu, W.J. Zhou, R. Ahmed, A.G. Hu, X.H. Guo, M. A. Cohen Stuart, Controlling morphology and release behavior of sorafenib-loaded nanocarriers prepared by flash nanoprecipitation, *Ind. Eng. Chem. Res.* 57 (35) (2018) 11911–11919.

[22] Y. Liu, G.Z. Yang, D. Zou, Y. Hui, K. Nigam, A.P.J. Middelberg, C.X. Zhao, Formulation of nanoparticles using mixing-induced nanoprecipitation for drug delivery, *Ind. Eng. Chem. Res.* 59 (9) (2020) 4134–4149.

[23] S.L. Levit, H. Yang, C. Tang, Rapid self-assembly of polymer nanoparticles for synergistic codelivery of paclitaxel and lapatinib *via* flash NanoPrecipitation, *Nanomaterials (Basel)* 10 (3) (2020) 561.

[24] Z. Chen, Z.N. Fu, L. Li, E.G. Ma, X.H. Guo, A cost-effective nano-sized curcumin delivery system with high drug loading capacity prepared *via* flash nanoprecipitation, *Nanomaterials (Basel)* 11 (3) (2021) 734.

[25] M.E. Gindy, A.Z. Panagiotopoulos, R.K. Prud'homme, Composite block copolymer stabilized nanoparticles: Simultaneous encapsulation of organic actives and inorganic nanostructures, *Langmuir* 24 (1) (2008) 83–90.

[26] M. Akbulut, P. Ginart, M.E. Gindy, C. Theriault, K.H. Chin, W. Soboyejo, R.K. Prud'homme, Generic method of preparing multifunctional fluorescent nanoparticles using flash NanoPrecipitation, *Adv. Funct. Mater.* 19 (5) (2009) 718–725.

[27] Y.Z. He, R.D. Priestley, R. Liu, A one-step and scalable continuous-flow nanoprecipitation for catalytic reduction of organic pollutants in water, *Ind. Eng. Chem. Res.* 55 (37) (2016) 9851–9856.

[28] M.J. Yu, W.W. Zhang, Z.Q. Guo, Y.Z. Wu, W.H. Zhu, Engineering nanoparticulate organic photocatalysts *via* a scalable flash nanoprecipitation process for efficient hydrogen production, *Angew. Chem.* 133 (28) (2021) 15718–15725.

[29] X.J. Jia, Y.F. Yan, A.B. Kayitmazer, Y.S. Li, Y.S. Xu, Scalable yielding of highly stable polyelectrolyte-coated copper sulfide nanoparticles by flash nanoprecipitation for photothermal-chemotherapeutics, *Adv. Funct. Mater.* 31 (32) (2021) 2100452.

[30] J. Han, Z.X. Zhu, H.T. Qian, A.R. Wohl, C.J. Beaman, T.R. Hoye, C.W. Macosko, A simple confined impingement jets mixer for flash nanoprecipitation, *J. Pharm. Sci.* 101 (10) (2012) 4018–4023.

[31] Z.X. Zhu, P. Xu, G.K. Fan, N.N. Liu, S.Q. Xu, X.L. Li, H.G. Xue, C.H. Shao, Y.L. Guo, Fast synthesis and separation of nanoparticles *via in situ* reactive flash nanoprecipitation and pH tuning, *Chem. Eng. J.* 356 (2019) 877–885.

[32] Y. Liu, C. Cheng, Y. Liu, R.K. Prud'homme, R.O. Fox, Mixing in a multi-inlet vortex mixer (MIVM) for flash nano-precipitation, *Chem. Eng. Sci.* 63 (11) (2008) 2829–2842.

[33] H. Shen, S. Hong, R.K. Prud'homme, Y. Liu, Self-assembling process of flash nanoprecipitation in a multi-inlet vortex mixer to produce drug-loaded polymeric nanoparticles, *J. Nanoparticle Res.* 13 (9) (2011) 4109–4120.

[34] J. Tao, S.F. Chow, Y. Zheng, Application of flash nanoprecipitation to fabricate poorly water-soluble drug nanoparticles, *Acta Pharm. Sin. B* 9 (1) (2019) 4–18.

[35] M. Li, Y.S. Xu, J.L. Sun, M.W. Wang, D.H. Yang, X.H. Guo, H.Y. Song, S. Cao, Y.F. Yan, Fabrication of charge-conversion nanoparticles for cancer imaging by flash nanoprecipitation, *ACS Appl. Mater. Interfaces* 10 (13) (2018) 10752–10760.

[36] B. Qin, R.X. Yao, X.L. Zhao, H. Tian, Enhanced photochromism of 1, 2-dithienylcyclopentene complexes with metal ion, *Org. Biomol. Chem.* 1 (12) (2003) 2187–2191.

[37] Y.T. Tam, K.K. To, A.H. Chow, Fabrication of doxorubicin nanoparticles by controlled antisolvent precipitation for enhanced intracellular delivery, *Colloids Surf.. B Biointerfaces* 139 (2016) 249–258.

[38] Z.X. Zhu, Flash nanoprecipitation: Prediction and enhancement of particle stability *via* drug structure, *Mol. Pharm.* 11 (3) (2014) 776–786.

[39] M.P. Desai, V. Labhasetwar, E. Walter, R.J. Levy, G.L. Amidon, The mechanism of uptake of biodegradable microparticles in Caco-2 cells is size dependent, *Pharm. Res.* 14 (11) (1997) 1568–1573.

[40] K.M. Pustulka, A.R. Wohl, H.S. Lee, A.R. Michel, J. Han, T.R. Hoye, A.V. McCormick, J. Panyam, C.W. Macosko, Flash nanoprecipitation: Particle structure and stability, *Mol. Pharm.* 10 (11) (2013) 4367–4377.

[41] S.S. Song, F.Y. Xia, S.Q. Huang, X.M. Wang, Study on e-type delayed fluorescence of carbazole derivatives, *J. Suzhou Univ. Sci. Technol.* 36 (4) (2019) 28–34.

[42] Y.J. Zhan, S.T. Yang, L.F. Chen, Y.B. Zeng, L. Li, Z.Y. Lin, L.H. Guo, W. Xu, Ultrahigh efficient FRET ratiometric fluorescence biosensor for visual detection of alkaline phosphatase activity and its inhibitor, *ACS Sustainable Chem. Eng.* 9 (38) (2021) 12922–12929.